ACS APPLIED MATERIALS & INTERFACES

www.acsami.org Research Article

Dynamic Assembly of Strong and Conductive Carbon Nanotube/Nanocellulose Composite Filaments and Their Application in Resistive Liquid Sensing

Heather G. Wise, Hidemasa Takana, and Anthony B. Dichiara*

Cite This: *ACS Appl. Mater. Interfaces* 2023, 15, 36647−36656 Read Online

ACCESS | Metrics & More | Article Recommendations | Supporting Information

ABSTRACT: The continuous flow assembly of colloidal nanoparticles from aqueous suspensions into macroscopic materials in a field-assisted double flow focusing system offers an attractive way to bridge the outstanding nanoscale characteristics of renewable cellulose nanofibrils (CNFs) at scales most common to human technologies. By incorporating single-walled carbon nanotubes (SWNTs) during the fabrication process, high-performance functional filament nanocomposites were produced. CNFs and SWNTs were first dispersed in water without any external surfactants or binding agents, and the resulting nanocolloids were aligned by means of an alternating electric field combined with extensional sheath flows. The nanoscale orientational anisotropy was then locked by a liquid−gel transition during the materials assembly into macroscopic filaments, which greatly improved their mechanical, electrical, and liquid sensing properties. Significantly, these findings pave the way toward the environmentally friendly and scalable manufacturing of a variety of multifunctional fibers for diverse applications.

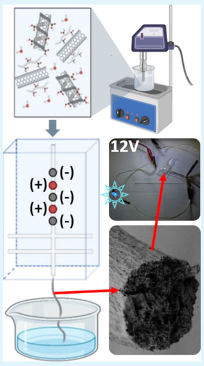

KEYWORDS: *nanocellulose, carbon nanotubes, filament composite, flow focusing, dielectrophoresis*

1. INTRODUCTION

The evolution of modern electronics toward miniaturization and flexibility becomes an essential aspect of the information and communication technology industry. In particular, the rapid proliferation of ever smarter and more feature-rich wearable devices is expected to have a significant impact upon most personal and business sectors, such as healthcare, sports, fashion, transportation, security, gaming, and infotainment.[1−4] The global market for flexible electronics was estimated at \$15.7 billion in 2020 and is projected to reach a revised size of \$44.8 billion by 2026, growing at a Compound Annual Growth Rate (CAGR) of 18.6% during the forecasted period.[5] However, without a sustainable design strategy, wearable electronics might just become another category of mass-consumed products contributing to global resource depletion. Wearable devices have already been adopted by 12.3% of the global population in 2020 and will reach up to 65.6% by 2030.[6] In addition, the frequency of replacing old devices also increases rapidly, stretching the demand for landfill space with the accumulation of persistent e-waste. A recent study revealed that every third American consumer who owned a wearable product stopped using it within six months, contributing a sizeable fraction of the 3.2 million tons of e-waste discarded annually in the U.S.[7] Considering the upcoming proliferation of wearables along with their short lifecycle, the development of renewable and biodegradable systems becomes essential.

This next generation of electronics will require enhanced portability, flexibility, multifunctionality, operational safety, energy autonomy, and biocompatibility, while reducing the cost and minimizing environmental impact. Cellulose is a naturally abundant renewable biomacromolecule that offers multiple advantages when extracted at the nanoscale, making it an ideal candidate for manufacturing sustainable and flexible wearables and electronics. As cellulose nanofibrils (CNFs) are becoming more readily available, it is critical to develop scalable processes that limit the occurrence of stochastic defects when assembling CNFs into macroscopic structures for applications at scales most common to human technologies. By combining the effects of shear and elongational forces and electrostatic torque exerted on a CNF suspension, we previously established the first-of-its-kind field-assisted flow focusing method capable of producing highly ordered macroscopic cellulose filaments in a flow-through process.[8] This technological accomplishment offers unique opportunities to design high-performance fibrous materials.

The present research reports on the incorporation of single-walled carbon nanotubes (SWNTs) to the filament composition, imparting conductivity to the resulting anisotropic composites and enabling resistive-sensing applications. Re-

Received: March 17, 2023
Accepted: June 27, 2023
Published: July 12, 2023

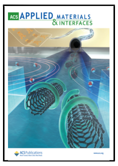

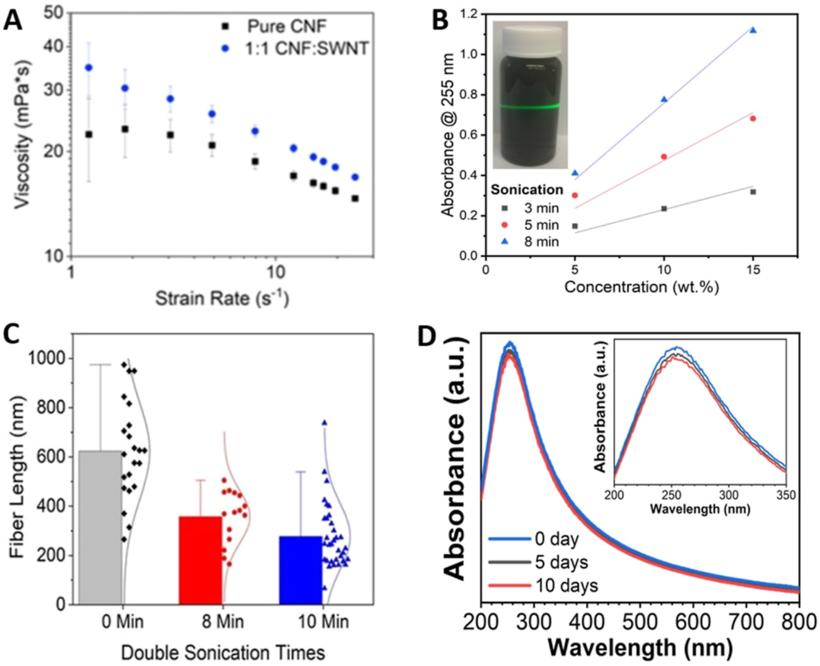

Figure 1. (A) Strain-rate dependence of the viscosity for aqueous dispersions of pure CNF and CNF/SWNT mixture after 8 min double sonication treatment. (B) Absorption spectra of aqueous suspensions comprising equal quantities of CNFs and SWNTs at varying solid concentrations. The inset shows a photo of the Tyndall effect demonstrating the colloidal nature of the aqueous CNF/SWNT dispersions at 15 wt % solid. (C) CNF length distribution as a function of sonication time. (D) Colloidal stability of the aqueous CNF/SWNT dispersion prepared at 15 wt % total solid content and 8 min sonication over a 10 day period. The inset shows the zoomed in view of the wavelength region ranging from 200 to 350 nm.

search combining nanocellulose with electrically conductive nanocarbons, such as carbon nanotubes (CNTs) or graphene, to form fibrous composites has been reported in the recent literature,[9−11] although studies involving CNFs remain scarce compared to other types of nanocellulose like cellulose nanocrystals (CNCs).[12] Previous reports typically show that while higher nanocarbon contents improve the composite's electrical conductivity, it often comes at the expense of its mechanical performance, since hydrophobic nanocarbons can disrupt the structural integrity of polar cellulose networks.[13] For instance, when CNT loading is above the percolation threshold, it can yield 4−10 orders of magnitude increase in conductivity; however, these results were accompanied by drastic reductions in tensile strength sometimes greater than 50%.[14−17] Therefore, most cellulose-based conductive composites maintained relatively low nanocarbon contents (*i.e.* a few wt %).

Preserving the mechanical integrity of composites at high filler contents requires strong interfacial interactions between fillers and matrix, as well as an even filler distribution with minimal aggregation to prevent localized stress and crack propagation.[18,19] Although covalent bonding can fortify the nanoparticle/matrix interface, the cross-linking reactions often sacrifice the composite's conductivity by altering the fillers' electronic structure.[20−22] Here, we leverage the ability of CNFs to form stable, colloidal dispersions with SWNTs in water without chemical functionalization or surfactants for the fabrication of strong and conductive filament nanocomposites. Although they are typically more expensive than their multi-walled counterparts, SWNTs are preferred here due to their aspect ratio that matches that of CNFs more closely. The complexation between CNFs and SWNTs is examined by near-field IR spectroscopy, which is an innovative analytical method rarely used for CNF characterization.[23] The CNF/SWNT nanocolloids are then aligned by means of an alternating electric field combined with elongational flows, while the nanoscale orientational anisotropy is locked by a liquid−gel transition during the materials assembly into macroscopic filaments (Figure 1A). To the best of our knowledge, this study consists of the first examination of dissimilar and polydisperse nanoparticles in a dynamic field-assisted flow-focusing system. The structural, mechanical, and electrical properties of the resulting filament nanocomposites are thoroughly assessed. In addition, as-fabricated materials are applied as ultra-sensitive-resistive liquid water sensors enabling the reliable detection of sub-μL volumes. Sensing small volumes of liquid water remains a difficult challenge because materials employed in current technologies have either weak responses due to their non-polar nature or they are partially soluble in water leading to their rapid degradation once wet. This work has important implications for the manufacturing of sustainable multifunctional materials with small form factors.

2. RESULTS AND DISCUSSION

2.1. Colloidal Dispersion of Aqueous CNF/SWNT Mixtures. Previous research has reported that TEMPO-oxidized CNFs with high aspect ratio and charge density are effective at dispersing aqueous CNTs at relatively high concentrations.[36] Here, CNFs were extracted from bleached softwood pulp based on our previously established TEMPO-mediated oxidation procedure followed by mechanical defibrillation.[24,25] The resulting CNFs had a charge density of 0.75 mmol COOH/g, as determined by conductometric titration and a high aspect ratio with a mean width and length of 2 and 625 nm, respectively, as measured by atomic force microscopy (Figure S1). As-synthesized CNFs were mixed with commercially available single-walled CNTs (SWNT, 5−30 μm length and 2−5 nm diameter) in different proportions.[26] Per the manufacturer specifications, the SWNTs contained 2.7% carboxylic groups and were purified to remove residual catalysts (>99% carbon purity) and amorphous carbon (<3 wt %). Note that few multiwall CNTs with a small number of graphitic layers (*i.e.* < 10) existed within the nanotube samples. Aqueous mixtures were prepared using a previously established double acoustic irradiation method to break the carbon nanomaterial aggregates while minimizing the extent of cavitation-induced damages to the nanoparticles.[27] The minimal change in the integrated intensity ratio of the G band to the D band (IG/ID), as determined by Raman spectroscopy (Figure S2), supports the low level of structural alteration inflicted to SWNTs during the double acoustic irradiation treatment. All dispersions behave like non-Newtonian fluids as the viscosity decreased when the strain rate increased (Figure 1A). The addition of SWNTs increased the solution viscosity despite the lubricating effect of nanotubes.[28] This might be attributed to the higher mass of the mixture and the reduced Coulombic stability of CNF/SWNT complexes compared to sole CNF particles.[29] The presence of SWNTs also enhanced the shear-thinning behavior of the mixture and expanded the shear-thinning region to low strain rates. Absorption spectroscopy revealed that CNF/SWNT suspensions were the most active in the UV−visible region, with a strong peak at 255 nm characteristic of the surface π-plasmon excitation of SWNTs (Figure 1B). Since bundled SWNT aggregates hardly absorb any light in the UV range, the 255 nm peak can be used to assess the degree of SWNT disentanglement.[30] The linear correlation between the absorption at 255 nm and the quantity of SWNTs in solution indicated the good dispersing action of CNFs for SWNTs in the [5−15 wt %] total solid concentration range and at a CNF/SWNT mass ratio of 1:1 w/w. Results also showed that longer sonication times improved the SWNT individualization at a given solid concentration. However, prolonging the nanoparticle exposure to double acoustic irradiation beyond 8 min had not significant effect on the degree of SWNT individualization (data not shown), but it kept decreasing the nanoparticle length (Figure 1C). This is consistent with previous studies reporting that CNTs suspended in water experienced extensive cutting after 5 min of horn sonication.[31] Therefore, a double sonication time of 8 min offered a good compromise to achieve both a high dispersion quality and a narrow nanoparticle length distribution, while preventing the shortening of nanoparticles by more than half of their initial size. The aqueous mixtures prepared under these conditions remained very stable over a 10 day period (Figure 1D), which corresponded to the maximum time within which the nanoparticle dispersions were implemented in the field-assisted flow focusing system. To perform this colloidal stability test, 20 mL samples were stored in the dark at room temperature without any treatment or agitation and periodical absorbance measurements were taken over a 10 day period by pipetting 3.5 mL aliquots to quartz cuvettes. Photographs of the aqueous CNF/SWNT dispersions at the 0-, 5- and 10 day points are shown in Figure S3.

2.2. Nanoparticle Complexation. Two mechanisms have been reported in the literature to describe the complexation between CNFs and CNTs—namely, a wrapping effect[32,33] and counterion interactions.[34,35] The former, which consists of the physical entanglement between CNFs and CNTs, has been suggested based on the comparison of diverse components' height identified from speculated differences in length and measured by AFM.[36] The latter, involving the delocalization of electrons in the sp^2 carbon lattice of CNTs induced by the fluctuation of counterions on the CNF surface, has been proposed based on observations made with a spherical AFM probe coated with CNFs and brought into proximity of a graphene sheet.[34] The colloidal dispersion of the resulting CNF/CNT complexes is then established by electrostatic stabilization originating from the anionic nature of CNF in aqueous solution. Here, nano-FTIR microscopy, which is a relatively novel multimodal technique applying the AFM enhancement of near-field infrared radiation for chemical analysis at the nanoscale, was employed to probe the association between CNFs and SWNTs (Figure S4). The method uses the forces exerted on the AFM tip via the light-induced tip−sample interaction to provide a direct image of the specimen, while simultaneously combining the exaltation of the field between the tip and the sample to enable infrared spectroscopy analysis at spatial resolution well below the diffraction limit. Several spectra were recorded at various locations along the length of a single nanoparticle (*i.e.* presumably SWNT based on length differences) where multiple crossings with other particles (*i.e.* most likely CNFs) occurred (Figure 2A,B). The variations in intensity of characteristic cellulose bands centered around 1071, 1100, and 1347 cm^{-1} confirmed the presence of CNFs at the particle crossing points (Figure 2C).[37,38] Notably, a broadening of the peak at 1612 cm^{-1}, which is attributed to unsaturated structures, suggested that aromatic interactions exist between the nanoparticles.[39] The changes in intensity of the feature at 1710 cm^{-1}, assigned to carbonyl (C═O) stretching in carboxylic acid groups,[40] might indicate the presence of hydrogen bonding between CNFs and SWNTs. The strong bonding interactions between CNFs and SWNTs were further demonstrated by the red-shifts observed in the graphitic D- and G-bands during Raman spectroscopy analysis (Figure S2). These results are consistent with previous reports postulating that hydrophobic interactions occur between the aromatic

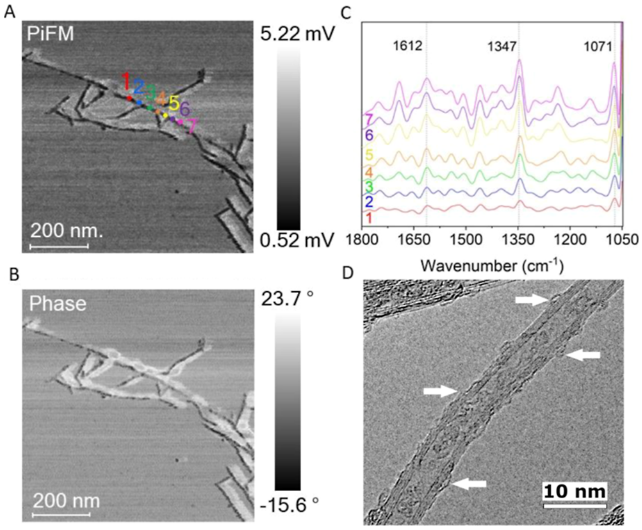

Figure 2. PiFM (A) and phase (B) images of aqueous CNF/SWNT dispersions at 1:1 mass ratio drop casted onto freshly cleaved mica substrates. (C) Stacked PiFM spectra from the different color-coded regions highlighted in (A). (D) TEM micrograph of a CNF-wrapped carbon nanotube with arrows highlighting the locations of interparticle entanglement.

https://doi.org/10.1021/acsami.3c03906
ACS Appl. Mater. Interfaces 2023, 15, 36647−36656

CNF primary backbone and the SWNT wall.[34,36] To further verify whether the ultrasonic agitation could lead to physical interparticle entanglement, the CNF/SWNT mixtures were aliquoted immediately after sonication and dropped onto copper grids (S162, Plano GmbH, Wetzlar/Germany) for transmission electron microscope (TEM) analysis. Prior to TEM imaging, the copper grids were placed on a tissue to remove the water instantly and fix the state of dispersion by limiting particle agglomeration. The TEM analysis showed evidence of sonication-induced interparticle entanglement, as indicated by the white arrows in Figure 2D. The multi-point non-covalent interactions between CNFs and the SWNT surface promote the wrapping dispersion effect.

2.3. Structural Characterization of Filament Nanocomposites. Unless otherwise specified, aqueous mixtures of CNFs and SWNTs at a mass ratio of 1:1 were used to produce filament nanocomposites, while pristine CNF filaments were also fabricated for comparison purposes, as depicted in Figure 3. The as-prepared nanoparticle dispersions were fed into a 1 mm microfluidic channel equipped with five circular copper electrodes followed by two sets of extensional flows using a similar field-assisted flow focusing process as described elsewhere.[8] An alternating AC electrical field of 100 V_{pp} was applied to improve the ordering of the nematic phase. The dissociation level of polar groups on the surface of colloidal nanoparticles can be influenced by the solution pH to trigger the formation of a solid hydrogel. Therefore, upon contact with 1 M HCl at the second extensional flow, the added protons neutralize the charge on the nanoparticle surface. In particular, the protonation of the carboxyl groups at low pH decreases both the surface potential and electrostatic repulsion of CNF. When insufficient charge repulsion is present, Van der Waals attraction forces become dominant, allowing the nanoparticles to come in close with each other, initiating the electrostatic-driven gelation of the material. The resulting hydrogel threads were then continuously extruded at a rate of 0.7 $cm \cdot s^{-1}$ into a bath of deionized water and dried at room temperature prior to further analysis. Scanning electron microscopy revealed that all filaments, regardless of SWNT content and applied voltage, had a similar mean diameter of 11.5 μm and exhibited a uniform and tightly packed core structure with no obvious voids (Figure 4A,B). Observations of cryo-fractured sections of the filament nanocomposites at higher magnification revealed the presence of tightly packed nanoparticles evenly distributed throughout the entire filament core with an obvious alignment along the longitudinal direction. The external surface of the composite filaments exhibited a rough and bumpy texture comparable to that of pure CNF specimens (Figure S5). Conductive SEM imaging techniques further highlighted the presence of SWNTs beneath the filament surface (Figure 4C), which appeared to be oriented parallel to the filament's long axis. Subsurface SWNT chaining was obvious for the filament nanocomposites prepared under an applied voltage of 100 V_{pp}, which is a common characteristic of the dielectrophoretic alignment of nanoparticles.[41,42] This means that the damping action caused by the higher viscosity of the CNF/SWNT mixture was not sufficient to oppose the effect of the electrostatic torque on nanoparticle alignment. Moreover, the red shift and broadening of the hydroxyl and carboxyl FTIR signatures at 3330 and 1600 cm^{-1} (Figure 4D) demonstrated that hydrogen bonding still existed between CNFs and SWNTs after the gelation of colloidal nanoparticles into macroscopic filaments. These observations of a combined organized microstructure and strong interfacial interactions between CNFs and SWNTs are expected to lead to consistent hybrid filament formation and good transfer of mechanical properties across scales.[43]

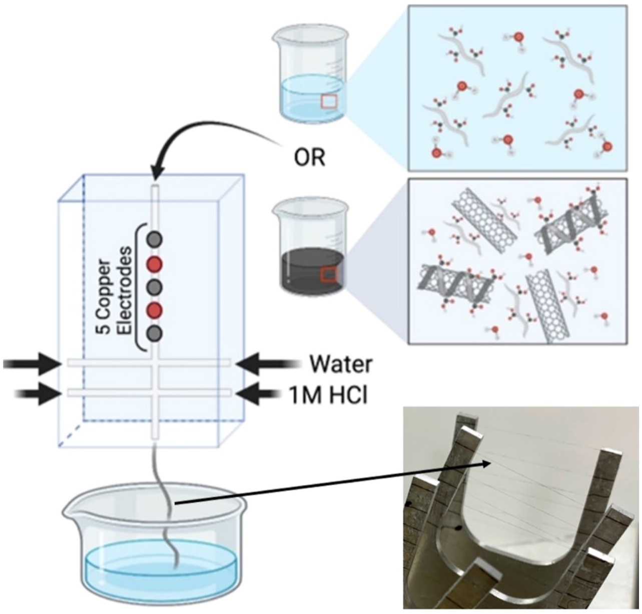

Figure 3. Diagram of the field-assisted flow-focusing system employed for the continuous fabrication of macroscopic nanocellulose structures with a photograph of as-produced electrically conductive filament nanocomposites.

2.4. Mechanical and Electrical Properties of Filament Nanocomposites. The strength properties of filament nanocomposites prepared with various SWNT contents (*i.e.* 0, 15, 25, and 50 wt %) and under different electric fields (*i.e.* 0 and 100 V_{pp}) were examined using a uniaxial tensile tester, as depicted in Figure 5. For SWNT contents of 15 wt % or below, the applied voltage did not affect the mechanical performance and the tests at 100 V_{pp} did not show any significant differences compared to the ones conducted without electric field (Figure 5B). At higher SWNT loadings, however, the effect of the applied voltage on the filaments' mechanical characteristics became statistically significant with an increase (when the electric field was set to 100 V_{pp} compared to when it was turned off) in strength of 31 and 16% and in Young's modulus of 33 and 13% on average at 25 and 50 wt % SWNTs, respectively (Figure 5C). Interestingly, the mechanical properties of hybrid filaments gradually increased as the level of SWNTs rises. Such observations are unprecedented in the literature, where higher CNT loadings in cellulose-based composites typically induce a reduction in strength due to (i) the non-polar nature of CNTs, disrupting inter-cellulose bonding, and to (ii) the easier nanoparticle slippage promoted by weak interactions between CNT aggregates.[9,34,36,44] These negative effects can be uniquely counterbalanced by the enhanced microstructure ordering achieved at higher SWNT contents owing to the combined action of electrostatic torque and hydrodynamic flow toward orientational anisotropy. Since electric fields below 100 V_{pp} were previously reported to have a negligible effect on the nematic ordering of CNFs alone (Figure S6),[8,45] the presence of SWNTs in sufficient quantities is expected to play a pivotal role in the preferred orientation of the filament microstructure. First, the delocalized π-electron

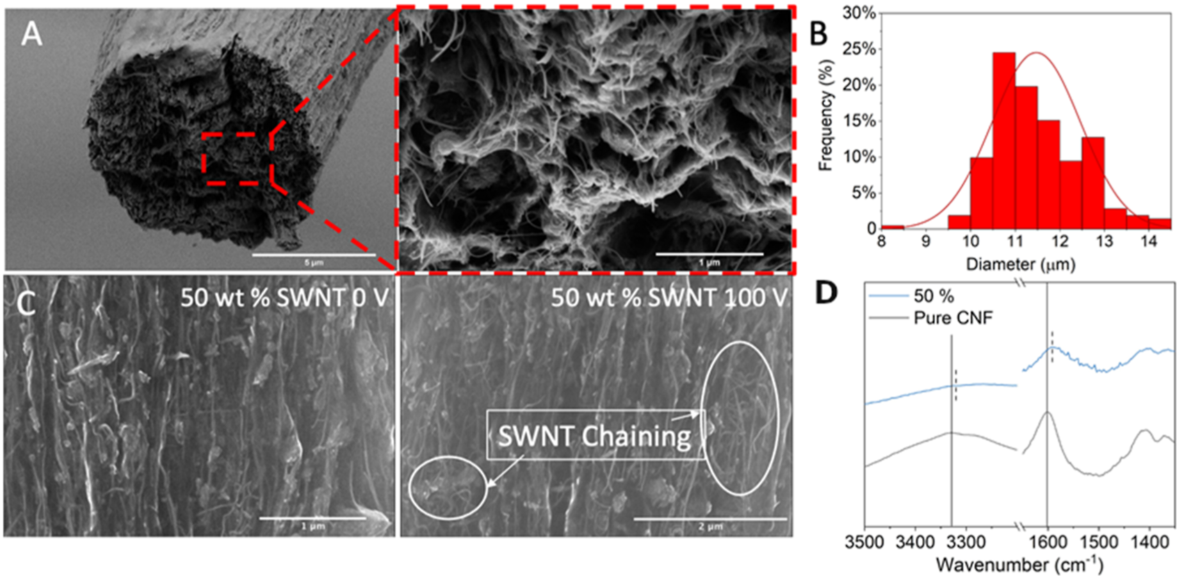

Figure 4. (A) Representative SEM images showing the cross-section of a cryo-fractured filament comprising 50 wt % SWNTs at low and high magnifications. (B) Diameter distribution of filament nanocomposites prepared under various conditions. Both SWCNT content and applied voltage did not induce any statistical differences in the filament diameter. (C) Backscattered electron imaging of filament composites prepared at applied voltages of 0 and 100 V_{pp}. (D) FTIR spectra of nanocellulose filaments containing 0 and 50 wt % SWNTs. The vertical solid and dashed lines highlight the peak positions in the FTIR spectra of pure CNF and CNF/SWNT samples, respectively.

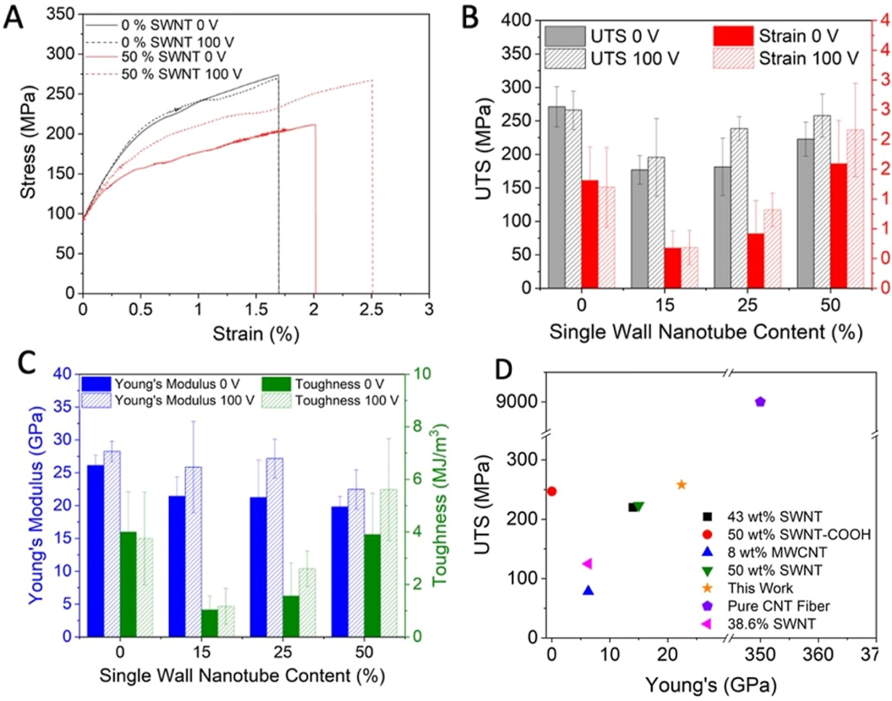

Figure 5. (A) Representative stress−strain curves of nanocellulose filaments containing 0 and 50 wt % SWNTs prepared at applied voltages of 0 and 100 V_{pp}. (B−C) Mechanical properties of hybrid filaments produced with and without electric field and at various SWNT contents. (D) Tensile strength and Young's modulus map comparing different CNF/CNT filaments reported in the literature.[9,34,36,44]

clouds of carbon nanotubes are expected to generate a stronger electric-field-induced polarization than the polar groups periodically occurring along the cellulose chains. Then, our previous numerical study demonstrated that while shorter fibrous particles exhibit a faster response to the electric field and align better, they also de-align more rapidly downstream of the electric field.[46] In addition, Brownian motion tends to limit the hydrodynamic flow alignment of shorter fibrous particles. Therefore, considering the estimated residency times of nanoparticles in the extensional flow region (*i.e.* 8.3 s) and in the applied electric field region (*i.e.* 150 s), the greater polarizability and length of SWNTs (*i.e.* few μm) compared to CNFs (*i.e.* few hundred nm) allow them to both align better along the electric field and hydrodynamic flow directions, and withstand orientation relaxation better until the gelation of the filament structure. The presence of SWNTs at 15 and 25 wt % in the filament composition decreased both the strength, stiffness, strain-to-failure, and toughness of the nanocomposites

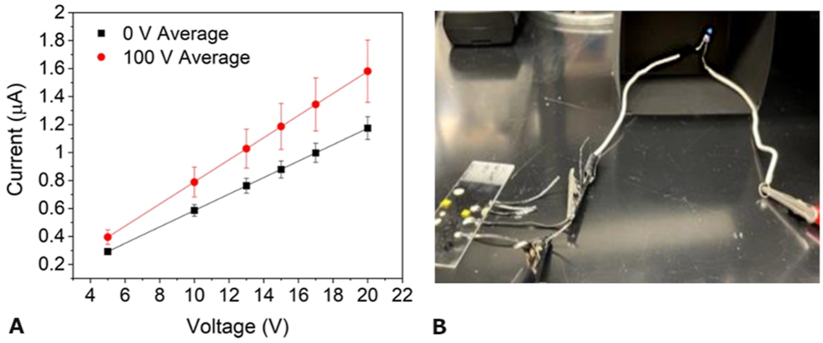

Figure 6. (A) $I-V$ curves of hybrid filaments containing 50 wt % SWNTs prepared at applied voltages of 0 and 100 V_{pp}. (B) Photograph of a LED operated using a single hybrid filament connected to a 12 V battery.

compared to pure CNF materials (Figure 5B,C). This loss in mechanical properties was recovered, at least partially, by the improved nanoparticle orientation at 50 wt % SWNT loading. Most notably, when the electric field was switched from 0 to 100 V_{pp}, the nanocomposite filaments comprising an equal proportion of CNFs and SWNTs achieved the same strength of ∼261 MPa than pure CNF filaments, while surpassing its toughness by more than 50%. Such simultaneous improvement in both strength and toughness is relatively seldom for this type of cellulose-based composites at high CNT contents (Figure 5D). When compared with other nanocomposite manufacturing methods previously reported in the literature, our tested filaments exhibited tensile strength values (*i.e.* 261 MPa) that are 3.6 times that of CNF/SWNT membranes (*i.e.* 73 MPa),[47] 2.5 times that of CNF/CNT filaments fabricated by interfacial nanoparticle complexation (*i.e.* 103 MPa),[48] and 2.3 times that of CNF/CNT filaments produced by wet spinning (*i.e.* 113 MPa).[44]

The beneficial effect of the electric field was also evident when looking at the electrical characteristics of the materials. Electrical measurements were conducted by mounting the as-prepared nanocomposite filaments onto glass slides using silver paste to minimize the contact resistance. Ohmic contacts were revealed from the linear trend that emerged from the current–voltage curves displayed in Figure 6A.[45] The resistance of the specimens containing the highest SWNT content considered in this work (*i.e.* 50 wt %) was reduced by more than 25% when the applied voltage was switched from 0 to 100 V_{pp}, which was sufficient to conduct enough current to operate a light-emitting diode (LED) when supplied with a 12 V battery (Figure 6B). Under the electric field, the nanoparticles became polarized and got attracted to each other by Coulombic interactions from the opposite charges present at their ends, forming a percolated network of electrically conductive SWNTs, hence lowering the resistance of the composite. This observation is consistent with previous studies on the dielectrophoretic alignment of CNTs, demonstrating that a gain in electrical conductivity is typically associated with materials exhibiting more organized microstructures.[26,49,50]

2.5. Ultrasensitive-Resistive Response to Liquid Water.

Prompted by the anisotropic hydroexpansion behavior of cellulose, we proposed to examine whether the higher ordering degree of the hybrid filaments comprising of 50 wt % SWNTs and prepared under an applied voltage of 100 V_{pp} may be advantageous for advanced liquid-sensing applications. To this aim, the sensitivity to liquid water of different filament nanocomposites was assessed by recording simultaneously the relative changes in their diameter and electrical resistance as a function of time upon drop-casting 1 μL of deionized water. The analysis was carried out with the filament-mounted slides using an inverted light microscope (Zeiss Axiolab) equipped with a digital camera (Zeiss Axiocam ERc5s) and fitted with a Keithley 2450 Source Measurement Unit, as illustrated in Figure 7. The anisotropic swelling of the cellulose filaments, observed in Figure 8A and supplementary Video S1, disrupted the electron transport within the SWNT network, resulting in an abrupt increase in resistance upon immediate wetting. Unlike SWNTs which do not experience obvious dimensional change in water, wet cellulose fibers typically expand radially rather than in the longitudinal direction. The CNF hydroexpansion results from the water penetration into the cellulose intra/interchain pores with interactions between polar water molecules and oxygen groups on the CNF surface, which occurs mainly in the amorphous regions of cellulose where larger numbers of free hydroxyl moieties are available.[51] To a lesser extent, the presence of free water molecules may also affect the interfiber spacing by disrupting hydrogen bonding between adjacent CNFs. Given the relative alignment of nanoparticles in the macroscopic structure, it makes sense that the filaments also expand in the out-of-plane direction. While the radial expansions of the filaments were fully reversed upon drying, the electrical resistances did not completely return to their initial levels. This hysteresis effect was found to fade away after a few wetting/drying cycles. Recently, Soderberg et al. also revealed that the conductivity of CNF composites could be fully recovered after exposing spent materials to humidity values below 5% RH.[11] The hydroexpansion behavior and liquid sensitivity of nanocomposite filaments prepared with and without external electrical field were compared, as shown in Figure 8B,C. In each case, the evolutions of the filament

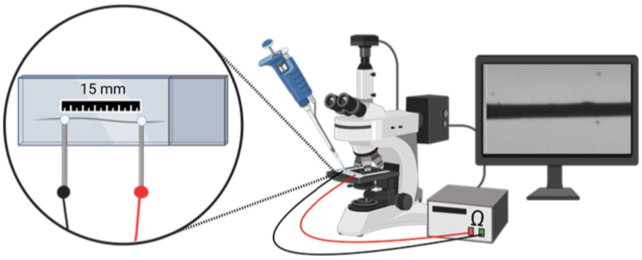

Figure 7. Schematic of the experimental set up used to measure simultaneously the variations in diameter and resistance of filament composites in the dry and wet states. Wetting involved drop casting 1 μL of deionized water onto the center position of the filament between the two electrodes.

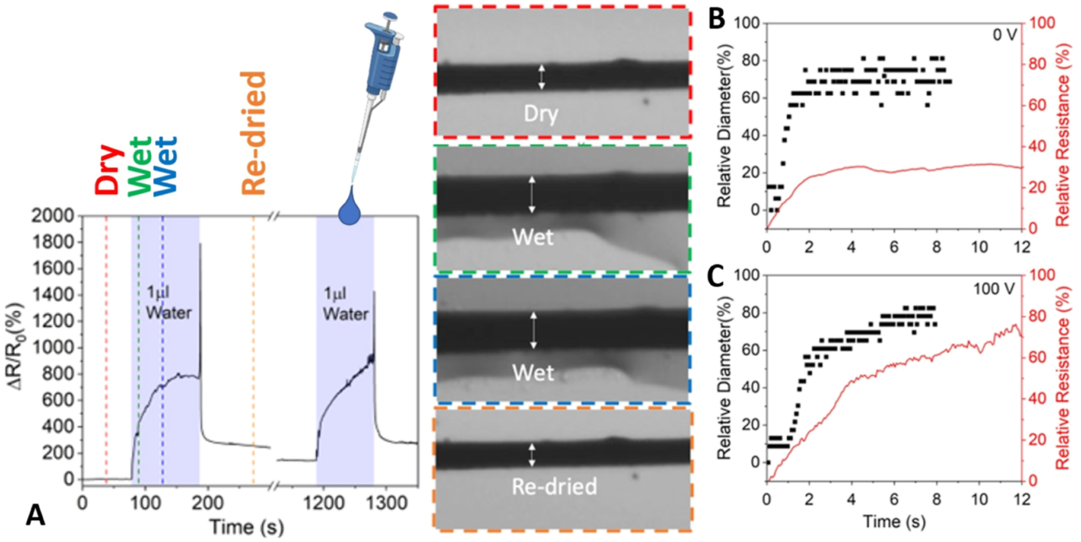

Figure 8. (A) Optical microscope images taken at the same 200× magnification depicting the swelling of a 50 wt % CNF/SWNT filament upon contact with 1 μL deionized water. The color-coded vertical lines in the graph showing the relative resistance of the filament composite over two successive wetting/drying cycles correspond to the times at which the various optical micrographs were taken. Note that the highlighted regions in the graph represent the wet stages of the analysis. Evolution of the relative resistance and diameter of filament composites comprising 50 wt % SWNT prepared in the absence (B) and in the presence (C) of a 100 Vpp voltage.

diameter and relative resistance were similar with both specimens presenting the same linear increase at very short times (*i.e.* <4 s). These initial trends were followed by a secondary increase at a slower rate both in diameter and resistance for the filaments prepared under an applied voltage of 100 V_{pp}. These observations are consistent with the swelling behavior of other cellulosic materials, which are commonly understood to demonstrate two distinct swelling phases when immersed in water: an initial short but fast phase where the swelling rate reaches a maximum, followed by a longer and slower phase where the swelling rate approaches zero.[52] For the filaments produced in the absence of electric field, a plateau was reached rapidly after the initial linear response, which might be attributed to the lower ordering degree of these samples. All filaments exhibited a maximum augmentation in their relative diameter of approximately 80% (Figure 8B) with a swelling rate of 60%·s^{-1} (Figure 8C) regardless of the voltage applied. Despite similar hydroexpansion characteristics, the filaments prepared at an applied voltage of 100 V_{pp} showed more than 2 times greater sensitivity compared to those fabricated in the absence of electric field. The improved nanoparticle orientation in this material enabled a record sensitivity of 800% after being wetted with only 1 μL for 2 min, which is nearly five times higher than our previously reported ultrasensitive paper sensors under similar wetting conditions.[52] Although benchmarking the liquid-sensing performance is quite challenging due to the varying experimental conditions (*i.e.* volume and composition of water, temperature, etc.) listed in the literature, comparable sensitivities have been reported when the sensory materials were soaked in water for extended time.[13,44,53]

3. CONCLUSIONS

In summary, pristine CNF and composite CNF/SWNT macroscopic filaments were produced by a scalable field-assisted double flow focusing method at ambient temperature and using nontoxic water as solvent. The presence of SWNTs yielded commendable enhancements in the mechanical and electrical characteristics of hybrid filaments, especially when an alternating electric field of 100 V_{pp} was applied during fabrication. The applied voltage was significantly lower than what is typically required to generate observable changes in the properties of pristine CNF filaments. Notably, the filament composites comprising 50 wt % SWNT exhibited superior Young's modulus and tensile strength than other similar materials reported in the literature, with values of 23 GPa and 261 MPa, respectively. The self-assembled nanostructured filament composites were further demonstrated to possess great potential in sensing of liquid water, with nearly 3 orders of magnitude change in their electrical resistance after being in contact with 1 μL water for only few minutes. This research paves the way toward the design of other multifunctional filaments comprising a variety of nanoparticles.

4. METHODS

4.1. Materials and Chemicals. Bleached Kraft softwood pulp, comprising a mixture of Douglas fir (*Pseudotsuga menziesii*) and Western Hemlock (*Tsuga heterophylla*), was kindly supplied by the WestRock mill in Tacoma, WA. Carboxyl-functionalized single-walled CNTs (>99% carbon purity) with respective length and diameter in the [5−30] μm and [2−5] nm ranges were purchased from Cheap Tubes Inc. in Grafton, VT. Sodium bromide (NaBr, 99+%), sodium hypochlorite (NaClO, 12.5 w/w %), hydrochloric acid (HCl, 1 M), and sodium hydroxide (NaOH, 1 M) were purchased from Fischer Scientific, while 2,2,6,6-tetramethylpiperidine (TEMPO, >98%) was obtained from Tokyo Chemical Industry Co. All the analytical grade reagents were used without further purification as received from the suppliers.

4.2. CNF Synthesis. CNFs were synthesized from Kraft pulp based on a previously described TEMPO-mediated oxidation process followed by mechanical defibrillation using an ultrasonic probe.[24,25] Briefly, the pulp was mixed in an aqueous solution containing TEMPO (9.5 mg·mL^{-1}), sodium bromide (10 w/w %), and sodium hypochlorite (5 mmol·g^{-1} pulp). Sodium hydroxide (1 M) was added dropwise to the mixture to stabilize the solution pH at 10. The reaction was stopped after 120 min by adjusting the solution pH to neutral using 1 M HCl. The suspension was then centrifuged at 5000 rpm for 15 min (Allegra 25R Centrifuge, Beckman Coulter) and the precipitate was dialyzed against deionized water for five days. The dialyzed solution was blended for 30 min and sonicated for an additional 2 min using a Sonics Vibracell VCX750 operated at 100% amplitude. The resulting dispersion was centrifuged at 5000 rpm for 15 min and the supernatant was stored for further characterization and processing. The length and diameter of as-synthesized CNFs were determined using an Asylum Research Cypher atomic force microscope (AFM) equipped with Arrow UHF probes, while the carboxylate content was measured by conductometric titration using a Cole-Palmer Oakton CON 6+ water quality meter based on a previously established procedure.[24,25]

4.3. Characterization of Colloidal Dispersions. A previously established double acoustic irradiation procedure was employed to mix the CNFs and SWNTs in deionized water in various proportions.[27] All double sonicated mixtures were centrifuged for 45 min at 5500 rpm to remove nanoparticle aggregates prior to further testing. As-prepared aqueous CNF/SWNT dispersions were then characterized by absorption spectroscopy within the [250−800] nm range with a 1 nm resolution using a PerkinElmer Lambda 750 spectrophotometer, and by transmission electron microscopy using a Tecnai G2 F20 SuperTwin TEM operated at a 200 kV accelerating voltage. The viscosity of the mixtures was measured at a constant temperature of 293 K using a DV2TLV viscometer from Brookfield fitted with a ULA spindle. The extent of sonication-induced cutting was assessed by measuring the nanoparticle length after different treatment conditions using an Asylum Research Cypher AFM equipped with ArrowUHF probes and operated in tapping mode at a scan rate of 1 Hz. Samples were prepared by drop casting 0.0005 wt % nanoparticle dispersions onto freshly cleaved Mica discs (TedPella Inc., 12 mm) and dried at room temperature under nitrogen atmosphere for 2 h prior to imaging. To ensure statistical soundness, a minimum of 25 measurements was collected for each sample and the results were subjected to Tukey tests with statistical differences in nanoparticle length being determined based on p-values <0.05 at a 5% alpha level (*i.e.* 95% confidence). The chemical interactions between CNFs and SWNTs were probed by nano-FTIR spectroscopy. The IR photo-induced force microscopy (PiFM, Molecular Vista) data were collected within the [750−1870] cm^{-1} range using a VistaScope from Molecular Vista Inc. couple to a LaserTune LT-OEM. Nano-FTIR signals outside of the above wavenumber range were not recorded due to higher noise levels induced by the lower laser energy at lower and higher frequencies. The PiFM analysis was conducted by operating the AFM in tapping mode using a μmasch NCH−Pt 300 kHz non-contact cantilever from Nanosensors.

4.4. Macroscopic Filament Preparation and Characterization. Filament composites were prepared by feeding the aqueous CNF/SWNT mixtures into a field-assisted double flow focusing system. The specifications of the microfluidic channel are reported in Figure S7 and the operating conditions were adjusted from our previous research.[8] Briefly, the aqueous colloidal dispersions were fed into a 1 × 1 mm^2 channel at a flow rate of 2.4 $mL{\cdot}h^{-1}$. Five 2 mm diameter copper electrodes spaced by 10 mm were set along the channel and supplied with an AC sinusoidal voltage from a function generator, which was then amplified using a high-voltage amplifier. The first pair of deionized (DI) water sheath flows was located 3 mm downstream from the bottom of the last electrode. The DI water sheath flow rates were adjusted to 6 $mL{\cdot}h^{-1}$ using syringe pumps. The second pair of sheath flows was positioned 3 mm downstream from the first one and supplied 1 M hydrochloric acid at a flow rate of 3.6 $mL{\cdot}h^{-1}$. The gel-like materials were collected in a DI water container 45 mm downstream of the second pair of sheath flows. As-produced filaments were cut to 30 mm sections and mounted on sample holders for drying in an oven operated at 60 °C for 24 h prior to further testing.

The filament morphology was examined by electron microscopy with a ThermoFisher Scientific Apreo SEM. Surface and cross-section topography images were taken using the in-chamber Everhart−Thornley detector at a 2 kV accelerating voltage, while subsurface micrographs were obtained using the in-column secondary e^- (SE) detector at an accelerating voltage of 20 kV. The chemical characteristics of the filaments were assessed by Fourier transform infrared spectroscopy within the [1100−3500] cm^{-1} wavenumber range and with a resolution of 1 cm^{-1} using a Shimadzu spectrophotometer operated in attenuated total reflectance (ATR) mode.

The mechanical properties of the filaments were assessed by performing tensile tests at a 0.5 $mm{\cdot}min^{-1}$ drawing rate using a Shimadzu EZ-SX uniaxial tester equipped with a 1 N load cell. The samples' cross-section was assumed to be circular, and the diameter was determined by electron microscopy analysis. For statistical soundness, a minimum of 25 replicates were conducted for each sample.

The current−voltage (I−V) curves of 30 mm long composite filaments with Ag paste were collected with a Keithley 2450 source meter unit using a two-probe configuration at a constant temperature and moisture of 23 °C and 50% relative humidity, respectively. The reported values and standard deviations correspond to averages of at least five measurements.

Swelling rate measurements were performed in real-time by mounting the filaments on a glass slide placed on a Zeiss Axiolab light microscope equipped with a Zeiss Axiocam ERc5s digital camera. Videos were recorded to show the active changes in the filament diameter upon dropping 1 μL deionized water onto the samples. Frames were extracted from the videos at a 0.7 s interval using Kinovea software, and Image J was employed to compute the filament diameter in each frame. The evolution of the samples' electrical resistance was also collected in situ during the swelling analysis by attaching a Keithley 2450 source meter unit. The relative change in resistance was calculated by dividing the difference between the wet and dry resistances over the initial resistance of the sample in its dry state.

■ ASSOCIATED CONTENT

Supporting Information

The Supporting Information is available free of charge at https://pubs.acs.org/doi/10.1021/acsami.3c03906.

Conductometric titration and AFM characterization of TEMPO-oxidized CNF, Raman spectra of SWNT before and after double acoustic irradiation treatment, photographs of aqueous CNF/SWNT dispersions, SEM imaging and 2D XRD analysis of pristine CNF filaments, and information about the field-assisted double flow focusing system (PDF)

Swelling behavior of a wet hybrid filament (MP4)

■ AUTHOR INFORMATION

Corresponding Author

Anthony B. Dichiara − *School of Environmental & Forest Sciences, University of Washington, Seattle, Washington 98195, United States;* orcid.org/0000-0002-3118-7029; Email: abdichia@uw.edu

Authors

Heather G. Wise − *School of Environmental & Forest Sciences, University of Washington, Seattle, Washington 98195, United States;* orcid.org/0000-0002-7627-1048

Hidemasa Takana − *Institute of Fluid Science, Tohoku University, Sendai 980-8577, Japan;* orcid.org/0000-0002-4862-9866

Complete contact information is available at: https://pubs.acs.org/10.1021/acsami.3c03906

Author Contributions

H.G. Wise: Methodology, Investigation, Data curation, Visualization, Writing—Original draft preparation. **H. Takana**:

Funding acquisition, Resources, Writing—Reviewing and Editing. **A.B. Dichiara**: Conceptualization, Supervision, Funding acquisition, Project administration, Resources, Writing—Reviewing and Editing.

Notes

The authors declare no competing financial interest.

■ ACKNOWLEDGMENTS

This research was supported by the NSF Advanced Manufacturing program (grant# 1927623), the McIntire-Stennis Cooperative Forestry Research Program (grant# 1020630) from the USDA National Institute of Food and Agriculture, the JSPS Kakenhi Program (grant# 22H01393), and the JSPS Core-to-Core Program (grant# JPJSCCA20210005). The present work was carried out under the University of Washington-Tohoku University: Academic Open Space and under the Collaborative Research Project of the Institute of Fluid Science, Tohoku University.

■ REFERENCES

(1) Aroganam, G.; Manivannan, N.; Harrison, D. Review on Wearable Technology Sensors Used in Consumer Sport Applications. *Sensors* **2019**, *19*, 1983.

(2) Wearable Sensors and Equipment in VR Games: A Review. springerprofessional.de. https://www.springerprofessional.de/en/wearable-sensors-and-equipment-in-vr-games-a-review/16680966 (accessed May 17, 2022).

(3) He, T.; Wang, H.; Wang, J.; Tian, X.; Wen, F.; Shi, Q.; Ho, J. S.; Lee, C. Self-Sustainable Wearable Textile Nano-Energy Nano-System (NENS) for Next-Generation Healthcare Applications. *Adv. Sci.* **2019**, *6*, 1901437.

(4) Khan, S.; Parkinson, S.; Grant, L.; Liu, N.; Mcguire, S. Biometric Systems Utilising Health Data from Wearable Devices: Applications and Future Challenges in Computer Security. *ACM Comput. Surv.* **2020**, *53*, 85.

(5) Clerck, J.-P. D. Wearables market outlook 2020: drivers and new markets. i-SCOOP. https://www.i-scoop.eu/wearables-market-outlook-2020-drivers-new-markets/(accessed May 17, 2022).

(6) Ometov, A.; Shubina, V.; Klus, L.; Skibińska, J.; Saafi, S.; Pascacio, P.; Flueratoru, L.; Gaibor, D. Q.; Chukhno, N.; Chukhno, O.; Ali, A.; Channa, A.; Svertoka, E.; Qaim, W. B.; Casanova-Marqués, R.; Holcer, S.; Torres-Sospedra, J.; Casteleyn, S.; Ruggeri, G.; Araniti, G.; Burget, R.; Hosek, J.; Lohan, E. S. A Survey on Wearable Technology: History, State-of-the-Art and Current Challenges. *Comput. Networks* **2021**, *193*, 108074.

(7) Arain, A. L.; Pummill, R.; Adu-Brimpong, J.; Becker, S.; Green, M.; Ilardi, M.; Van Dam, E.; Neitzel, R. L. Analysis of E-Waste Recycling Behavior Based on Survey at a Midwestern US University. *Waste Manag.* **2020**, *105*, 119−127.

(8) Wise, H. G.; Takana, H.; Ohuchi, F.; Dichiara, A. B. Field-Assisted Alignment of Cellulose Nanofibrils in a Continuous Flow-Focusing System. *ACS Appl. Mater. Interfaces* **2020**, *12*, 28568−28575.

(9) Wan, Z.; Chen, C.; Meng, T.; Mojtaba, M.; Teng, Y.; Feng, Q.; Li, D. Multifunctional Wet-Spun Filaments through Robust Nanocellulose Networks Wrapping to Single-Walled Carbon Nanotubes. *ACS Appl. Mater. Interfaces* **2019**, *11*, 42808−42817.

(10) Zhu, G.; Giraldo Isaza, L.; Huang, B.; Dufresne, A. Multifunctional Nanocellulose/Carbon Nanotube Composite Aerogels for High-Efficiency Electromagnetic Interference Shielding. *ACS Sustainable Chem. Eng.* **2022**, *10*, 2397−2408.

(11) Brett, C. J.; Forslund, O. K.; Nocerino, E.; Kreuzer, L. P.; Widmann, T.; Porcar, L.; Yamada, N. L.; Matsubara, N.; Månsson, M.; Müller-Buschbaum, P.; et al. Humidity-Induced Nanoscale Restructuring in PEDOT:PSS and Cellulose Nanofibrils Reinforced Biobased Organic Electronics. *Adv. Electron. Mater.* **2021**, *7*, 2100137.

(12) Li, K.; Clarkson, C. M.; Wang, L.; Liu, Y.; Lamm, M.; Pang, Z.; Zhou, Y.; Qian, J.; Tajvidi, M.; Gardner, D. J.; Tekinalp, H.; Hu, L.; Li, T.; Ragauskas, A. J.; Youngblood, J. P.; Ozcan, S. Alignment of Cellulose Nanofibers: Harnessing Nanoscale Properties to Macroscale Benefits. *ACS Nano* **2021**, *15*, 3646−3673.

(13) Dichiara, A. B.; Song, A.; Goodman, M.; He, D.; Bai, J.; Bai, J. Smart Papers Comprising Carbon Nanotubes and Cellulose Microfibers for Multifunctional Sensing Applications. *J. Mater. Chem. A* **2017**, *5*, 20161−20169.

(14) Mierczynska, A.; Mayne-L'Hermite, M.; Boiteux, G.; Jeszka, J. K. Electrical and Mechanical Properties of Carbon Nanotube/Ultrahigh-Molecular-Weight Polyethylene Composites Prepared by a Filler Prelocalization Method. *J. Appl. Polym. Sci.* **2007**, *105*, 158−168.

(15) Jimenez, G. A.; Jana, S. C. Electrically Conductive Polymer Nanocomposites of Polymethylmethacrylate and Carbon Nanofibers Prepared by Chaotic Mixing. *Composites, Part A* **2007**, *38*, 983−993.

(16) Mecklenburg, M.; Mizushima, D.; Ohtake, N.; Bauhofer, W.; Fiedler, B.; Schulte, K. On the Manufacturing and Electrical and Mechanical Properties of Ultra-High Wt.% Fraction Aligned MWCNT and Randomly Oriented CNT Epoxy Composites. *Carbon* **2015**, *91*, 275−290.

(17) Hornbostel, B.; Pötschke, P.; Kotz, J.; Roth, S. Single-walled carbon nanotubes/polycarbonate composites: basic electrical and mechanical properties. *Phys. Status Solidi B* **2006**, *243*, 3445−3451.

(18) Chen, J.; Liu, B.; Gao, X.; Xu, D. A Review of the Interfacial Characteristics of Polymer Nanocomposites Containing Carbon Nanotubes. *RSC Adv.* **2018**, *8*, 28048−28085.

(19) Xiang, D.; Harkin-Jones, E.; Linton, D.; Martin, P. Structure, Mechanical, and Electrical Properties of High-Density Polyethylene/Multi-Walled Carbon Nanotube Composites Processed by Compression Molding and Blown Film Extrusion. *J. Appl. Polym. Sci.* **2015**, *132*(), DOI: 10.1002/app.42665.

(20) Skákalová, V.; Dettlaff-Weglikowska, U.; Roth, S. Electrical and Mechanical Properties of Nanocomposites of Single Wall Carbon Nanotubes with PMMA. *Synth. Met.* **2005**, *152*, 349−352.

(21) Martinez-Rubi, Y.; Ashrafi, B.; Jakubinek, M. B.; Zou, S.; Laqua, K.; Barnes, M.; Simard, B. Fabrication of High Content Carbon Nanotube−Polyurethane Sheets with Tailorable Properties. *ACS Appl. Mater. Interfaces* **2017**, *9*, 30840−30849.

(22) Ma, P.-C.; Siddiqui, N. A.; Marom, G.; Kim, J.-K. Dispersion and Functionalization of Carbon Nanotubes for Polymer-Based Nanocomposites: A Review. *Composites, Part A* **2010**, *41*, 1345−1367.

(23) Kotov, N.; Larsson, P. A.; Jain, K.; Abitbol, T.; Cernescu, A.; Wagberg, L.; Johnson, C. M. Elucidating the fine-scale structural morphology of nanocellulose by nano infrared spectroscopy. *Carbohydr. Polym.* **2023**, *302*, 120320.

(24) Gu, J.; Hu, C.; Zhang, W.; Dichiara, A. B. Reagentless Preparation of Shape Memory Cellulose Nanofibril Aerogels Decorated with Pd Nanoparticles and Their Application in Dye Discoloration. *Appl. Catal., B* **2018**, *237*, 482−490.

(25) Goodman, S. M.; Che, J.; Neri, W.; Yuan, J.; Dichiara, A. B. Water-processable cellulosic nanocomposites as green dielectric films for high-energy storage. *Energy Storage Mater.* **2022**, *48*, 497−506.

(26) Sengezer, E. C.; Seidel, G. D.; Bodnar, R. J. Phenomenological Characterization of Fabrication of Aligned Pristine-SWNT and COOH-SWNT Nanocomposites via Dielectrophoresis under AC Electric Field. *Polym. Compos.* **2015**, *36*, 1266−1279.

(27) Goodman, S. M.; Ferguson, N.; Dichiara, A. B. Lignin-Assisted Double Acoustic Irradiation for Concentrated Aqueous Dispersions of Carbon Nanotubes. *RSC Adv.* **2017**, *7*, 5488−5496.

(28) Chen, L.; Xie, H.; Li, Y.; Yu, W. Nanofluids Containing Carbon Nanotubes Treated by Mechanochemical Reaction. *Thermochim. Acta* **2008**, *477*, 21−24.

(29) Lasseuguette, E.; Roux, D.; Nishiyama, Y. Rheological Properties of Microfibrillar Suspension of TEMPO-Oxidized Pulp. *Cellulose* **2008**, *15*, 425−433.

(30) Lauret, J.-S.; Voisin, C.; Cassabois, G.; Delalande, C.; Roussignol, Ph.; Jost, O.; Capes, L. Ultrafast Carrier Dynamics in Single-Wall Carbon Nanotubes. *Phys. Rev. Lett.* **2003**, *90*, 057404.

(31) Fuge, R.; Liebscher, M.; Schröfl, C.; Oswald, S.; Leonhardt, A.; Büchner, B.; Mechtcherine, V. Fragmentation Characteristics of Undoped and Nitrogen-Doped Multiwalled Carbon Nanotubes in Aqueous Dispersion in Dependence on the Ultrasonication Parameters. *Diamond Relat. Mater.* **2016**, *66*, 126−134.

(32) Sahoo, N. G.; Rana, S.; Cho, J. W.; Li, L.; Chan, S. H. Polymer Nanocomposites Based on Functionalized Carbon Nanotubes. *Prog. Polym. Sci.* **2010**, *35*, 837−867.

(33) Yang, L.; Zhang, B.; Liang, Y.; Yang, B.; Kong, T.; Zhang, L.-M. In Situ Synthesis of Amylose/Single-Walled Carbon Nanotubes Supramolecular Assembly. *Carbohydr. Res.* **2008**, *343*, 2463−2467.

(34) Hamedi, M. M.; Hajian, A.; Fall, A. B.; Håkansson, K.; Salajkova, M.; Lundell, F.; Wågberg, L.; Berglund, L. A. Highly Conducting, Strong Nanocomposites Based on Nanocellulose-Assisted Aqueous Dispersions of Single-Wall Carbon Nanotubes. *ACS Nano* **2014**, *8*, 2467−2476.

(35) Hajian, A.; Lindström, S. B.; Pettersson, T.; Hamedi, M. M.; Wågberg, L. Understanding the Dispersive Action of Nanocellulose for Carbon Nanomaterials. *Nano Lett.* **2017**, *17*, 1439−1447.

(36) Li, Y.; Zhu, H.; Wang, Y.; Ray, U.; Zhu, S.; Dai, J.; Chen, C.; Fu, K.; Jang, S.-H.; Henderson, D.; Li, T.; Hu, L. Cellulose-Nanofiber-Enabled 3D Printing of a Carbon-Nanotube Microfiber Network. *Small Methods* **2017**, *1*, 1700222.

(37) *Understanding PiF-IR Spectrum, Featuring Vista Series Microscopes*, Molecular Vista.

(38) Kesari, K. K.; O'Reilly, P.; Seitsonen, J.; Ruokolainen, J.; Vuorinen, T. Infrared Photo-Induced Force Microscopy Unveils Nanoscale Features of Norway Spruce Fibre Wall. *Cellulose* **2021**, *28*, 7295−7309.

(39) Rocha, S. M.; Goodfellow, B. J.; Delgadillo, I.; Neto, C. P.; Gil, A. M. Enzymatic Isolation and Structural Characterisation of Polymeric Suberin of Cork from Quercus Suber L. *Int. J. Biol. Macromol.* **2001**, *28*, 107−119.

(40) Guo, L.; Sato, H.; Hashimoto, T.; Ozaki, Y. FTIR Study on Hydrogen-Bonding Interactions in Biodegradable Polymer Blends of Poly(3-Hydroxybutyrate) and Poly(4-Vinylphenol). *Macromolecules* **2010**, *43*, 3897−3902.

(41) Gupta, P.; Rajput, M.; Singla, N.; Kumar, V.; Lahiri, D. Electric Field and Current Assisted Alignment of CNT inside Polymer Matrix and Its Effects on Electrical and Mechanical Properties. *Polymer* **2016**, *89*, 119−127.

(42) Amani, A. M.; Hashemi, S. A.; Mousavi, S. M.; Abrishamifar, S. M.; Vojood, A. *Electric Field Induced Alignment of Carbon Nanotubes: Methodology and Outcomes*; IntechOpen, 2017. DOI: 10.5772/intechopen.70481.

(43) Liu, Y.; Kumar, S. Polymer/Carbon Nanotube Nano Composite Fibers−A Review. *ACS Appl. Mater. Interfaces* **2014**, *6*, 6069−6087.

(44) Qi, H.; Schulz, B.; Vad, T.; Liu, J.; Mäder, E.; Seide, G.; Gries, T. Novel Carbon Nanotube/Cellulose Composite Fibers As Multifunctional Materials. *ACS Appl. Mater. Interfaces* **2015**, *7*, 22404−22412.

(45) Brouzet, C.; Mittal, N.; Rosén, T.; Takeda, Y.; Söderberg, L. D.; Lundell, F.; Takana, H. Effect of Electric Field on the Hydrodynamic Assembly of Polydisperse and Entangled Fibrillar Suspensions. *Langmuir* **2021**, *37*, 8339−8347.

(46) Takana, H.; Guo, M. Numerical simulation on electrostatic alignment control of cellulose nano-fibrils in flow. *Nanotechnology* **2020**, *31*, 205602.

(47) Luo, W.; Hayden, J.; Jang, S.-H.; Wang, Y.; Zhang, Y.; Kuang, Y.; Wang, Y.; Zhou, Y.; Rubloff, G. W.; Lin, C.-F.; Hu, L. Highly Conductive, Light Weight, Robust, Corrosion-Resistant, Scalable, All-Fiber Based Current Collectors for Aqueous Acidic Batteries. *Adv. Energy Mater.* **2017**, *8*, 1702615.

(48) Zhang, K.; Hujaya, S. D.; Jarvinen, T.; Li, P.; Kauhanen, T.; Tejesvi, M. V.; Kordas, K.; Liimatainen, H. Interfacial Nanoparticle Complexation of Oppositely Charged Nanocelluloses into Functional Filaments with Conductive, Drug Release, or Antimicrobial Property. *ACS Appl. Mater. Interfaces* **2020**, *12*, 1765−1774.

(49) Steinert, B. W.; Dean, D. R. Magnetic Field Alignment and Electrical Properties of Solution Cast PET−Carbon Nanotube Composite Films. *Polymer* **2009**, *50*, 898−904.

(50) Choi, E. S.; Brooks, J. S.; Eaton, D. L.; Al-Haik, M. S.; Hussaini, M. Y.; Garmestani, H.; Li, D.; Dahmen, K. Enhancement of Thermal and Electrical Properties of Carbon Nanotube Polymer Composites by Magnetic Field Processing. *J. Appl. Phys.* **2003**, *94*, 6034−6039.

(51) Botková, M.; Šutý, Š.; Jablonský, M.; Kucerkova, L.; Vrška, M. Monitoring of kraft pulps swelling in water. *Cellul. Chem. Technol.* **2013**, *47*, 95−102.

(52) Goodman, S. M.; Tortajada, I. A.; Haslbeck, F.; Oyulmaz, K. Y.; Rummler, A.; Sánchez, C. S.; Païs, J. T.; Denizli, H.; Haunreiter, K. J.; Dichiara, A. B. Scalable Manufacturing of Fibrous Nanocomposites for Multifunctional Liquid Sensing. *Nano Today* **2021**, *40*, 101270.

(53) Qi, H.; Mäder, E.; Liu, J. Unique water sensors based on carbon nanotube−cellulose composites. *Sens. Actuators, B* **2013**, *185*, 225−230.